

A new method for numerical inversion of the Laplace transform.

Bruno Hüpper and Eli Pollak

Chemical Physics Department, Weizmann Institute of Science, 76100 Rehovot, Israel

Abstract

A formula of Doetsch (*Math. Zeitschr.* **42**, 263 (1937)) is generalized and used to numerically invert the one-sided Laplace transform $\hat{C}(\beta)$. The necessary input is only the values of $\hat{C}(\beta)$ on the positive real axis. The method is applicable provided that the functions $\hat{C}(\beta)$ belong to the function space L_α^2 defined by the condition that $G(x) = e^{x\alpha}\hat{C}(e^x)$, $\alpha > 0$ has to be square integrable. This space includes sums of exponential decays $\hat{C}(\beta) = \sum_n^\infty a_n e^{-\beta E_n}$, e.g. partition functions with $a_n = 1$.

In practice, the inversion algorithm consists of two subsequent fast Fourier transforms. High accuracy inverted data can be obtained, provided that the signal is also highly accurate. The method is demonstrated for a harmonic partition function and resonant transmission through a barrier. We find accurately inverted functions even in the presence of noise.

I. INTRODUCTION

It is often relatively easy to compute the Laplace transform

$$\hat{C}(\beta) \equiv \int_0^\infty e^{-\beta E} \mathcal{C}(E) dE \tag{1.1}$$

of a function rather than the function itself. Similarly, it is often known how to compute a function on the imaginary axis and it is desirable to have a useful method for analytic continuation of the function to real time. Perhaps the most notable example is the computation of the propagator $\langle x|e^{-itH/\hbar}|x' \rangle$ which is very difficult because of the sign problem but which is straightforward in imaginary time $t = -i\hbar\beta$. A 'good' Laplace inversion methodology would solve both of these issues. The difficulty is that the inverse Laplace transform is known to be an ill-posed problem, since the addition of a small perturbation (for example $(\beta - 1 - ib)^{-1}$) to the image $\hat{C}(\beta)$ leads to a non-vanishing contribution (i.e. $\exp\{(1 + ib)E\}$) even in the limit of a very small perturbation (large b) [1].

Different numerical methods have been worked out to attempt at overcoming this problem [2], [3]. They divide roughly into five classes: The Fourier methods [4] which discretize the Bromwich inversion formula [5]

$$\mathcal{C}(E) = \frac{1}{2\pi} \int_{\sigma-i\infty}^{\sigma+i\infty} e^{\beta E} \hat{C}(\beta) d\beta. \tag{1.2}$$

This requires knowledge of the function in the complex plane and so does not really solve the problem.

The next two classes are based on the idea that the original function $\mathcal{C}(E)$ may be expanded into a basis set of functions whose transforms are known. To this category belong the linear least-squares fitting methods, where different basis sets are used, e.g. orthogonal polynomials [1,6], sums of exponentials [7,8], rational fractions or continued fractions [9], as well as others [10]. Nonlinear least-square fits are necessary if the signal is decomposed directly into a sum of exponentials with unknown decay rates E_n and coefficients a_n [11,12]. With both methods, it is difficult to treat signals accurately which are of the form $\hat{C}(\beta) =$

$\sum_{n=1}^{\infty} a_n e^{-E_n \beta}$. The Laplace transform of a polynomial-type basis possesses singularities and is inadequate for a fit to exponentials. On the other hand, an exponential with a non-integer decay-rate cannot correctly be approximated by exponentials of the sort $e^{-n\beta}$. As a result of these difficulties, these methods are able to give at most five exponentials. For other signals, such as rational polynomials, they have proved to be very accurate.

Another approach is the singular value decomposition method (SVD) [13,14] which is based on the theory of inverse problems. This method transfers the inverse Laplace transform into a matrix equation and the problem is transformed into the inversion of a nearly singular matrix, an ill-posed problem as well [15].

The fifth and most recent approach is the maximum entropy method [3,16]. In this method the entropy of the spectrum (which means in this context the number of ways of reproducing the spectrum) subject to a certain constraint is maximized. This approach allows to incorporate prior knowledge about the solution. Maximum entropy inversion is a nonlinear method, this complicates the practical application. However, it has proved its usefulness in recent computations, see for example Refs. [17–19]. The last two methods, maximum entropy and SVD, have recently been compared in simulating the electronic absorption spectrum of a chromophore coupled to a condensed phase environment and it turned out that the maximum entropy method is just able to reproduce the classical, smooth Franck-Condon contribution to the spectrum whereas SVD is capable of resolving finer oscillatory details [20].

In this paper we will resurrect an old formula, derived by Paley and Wiener [21] and by Doetsch [22], which is direct, there is no need to use a basis set and there is no need to solve a set of nonlinear equations. The Paley and Wiener form was rederived by Gardner et al. [23] 40 years ago and applied with limited success (due in part to computational limitations) to the analysis of multi-exponential decay curves. The old formulae were derived for functions $\hat{C}(\beta)$ which are L^2 integrable and so are not directly useful, for example for partition functions. We will generalize them, so that the method includes all functions which are L^2_α integrable, that is that the function $G(x) = e^{x\alpha} \hat{C}(e^x)$, $\alpha > 0$ is L^2 integrable. We

find for an exponential series that the quality of the inversion depends on the magnitude of the n -th exponent E_n . The smaller E_n , the more accurate the inversion. This enables to enhance the resolution of the inverted data.

In Section II, we derive the generalized Laplace inversion formula, numerical properties of the formula are discussed in Section III. The effect of shifting the signal is studied in Section IV. Applications to the harmonic oscillator partition function and a model resonant transmission probability are given in Section V. We end with a discussion of the merits of the method and outline some future extensions and applications.

II. THE CONTINUOUS SET \mathcal{L}_α^{-1} OF INVERSE LAPLACE TRANSFORMS

In this Section we derive and generalize a Laplace inversion formula which uses only the values of the Laplace transformed function $\hat{C}(\beta)$ on the positive, real β axis. The starting point is the one-sided Laplace integral Eq. (1.1) for which we perform a transformation of variables

$$E = e^\xi \quad \beta = e^x. \quad (2.1)$$

The motivation for this transformation, which goes back to Doetsch in 1936 [24], is to substitute the Laplace kernel $e^{-\beta E}$ in which we have the product of the two variables by a different one which contains the sum of the two variables. As a result, the Laplace integral takes the form of a convolution. If on both sides of the Laplace integral transform the Fourier transform is applied, a certain convolution theorem can be used in order to express the right hand side of the integral equation as a product of two terms. Finally, an algebraic manipulation leads to the desired inversion formula.

If we follow this route both sides of Eq. (1.1) are multiplied with an exponential $e^{x\alpha}$ with $\alpha > 0$ so that:

$$e^{x\alpha} \hat{C}(e^x) = \int_{-\infty}^{\infty} e^{\alpha(x+\xi)} e^{-e^{x+\xi}} \left[e^{\xi(1-\alpha)} \mathcal{C}(e^\xi) \right] d\xi \quad (2.2)$$

Now, the integrand on the right hand side consists of one part which depends only on the linear combination $x + \xi$ and a second, braced part which depends only on ξ . Next, both sides of the equation are Fourier transformed (with respect to x) and an application of the convolution theorem (which is equivalent to replacing the variable x by $z = x + \xi$) gives

$$\int_{-\infty}^{\infty} dx e^{ixy} e^{x\alpha} \hat{C}(e^x) = \int_{-\infty}^{\infty} d\xi \left[e^{\xi(1-\alpha)} \mathcal{C}(e^\xi) \right] e^{-i\xi y} \int_{-\infty}^{\infty} dz e^{-e^z} e^{\alpha z} e^{izy}. \quad (2.3)$$

The last integral can be written as

$$\int_{-\infty}^{\infty} dz e^{-e^z} e^{\alpha z} e^{izy} = \int_0^{\infty} dt t^{\alpha+iy-1} e^{-t} = \Gamma(\alpha + iy), \quad (2.4)$$

where $\Gamma(x)$ denotes the Gamma function [25]. Now, rearranging Eq. 2.2 leads to:

$$\int_{-\infty}^{\infty} d\xi \left[e^{\xi(1-\alpha)} \mathcal{C}(e^\xi) \right] e^{-i\xi y} = \frac{1}{\Gamma(\alpha + iy)} \int_{-\infty}^{\infty} dx e^{ixy} e^{x\alpha} \hat{C}(e^x), \quad (2.5)$$

Fourier transformation of both sides of Eq. 2.5 yields the inversion formula

$$\mathcal{C}(E = e^\xi) = \frac{e^{\xi(\alpha-1)}}{2\pi} \lim_{a \rightarrow \infty} \int_{-a}^a dy \frac{e^{i\xi y}}{\Gamma(\alpha + iy)} \int_{-\infty}^{\infty} dx e^{ixy} e^{x\alpha} \hat{C}(e^x). \quad (2.6)$$

Note that the inner integral in the inversion formula

$$g(y) = \int_{-\infty}^{\infty} dx e^{ixy} e^{x\alpha} \hat{C}(e^x) \quad (2.7)$$

has the symmetry property

$$g(-y) = \overline{g(y)}, \quad (2.8)$$

and the Gamma function obeys

$$\Gamma(\bar{z}) = \overline{\Gamma(z)}, \quad (2.9)$$

(where the bar denotes complex conjugation). This allows us to rewrite the inversion formula in a compact form as:

$$\begin{aligned} \mathcal{C}(E = e^\xi) &= \frac{e^{\xi(\alpha-1)}}{2\pi} \lim_{a \rightarrow \infty} \int_0^a dy \left(\frac{e^{i\xi y}}{\Gamma(\alpha + iy)} g(y) + \frac{e^{-i\xi y}}{\Gamma(\alpha - iy)} g(-y) \right) \\ &= \frac{e^{\xi(\alpha-1)}}{\pi} \operatorname{Re} \lim_{a \rightarrow \infty} \int_0^a dy \frac{e^{i\xi y}}{\Gamma(\alpha + iy)} \int_{-\infty}^{\infty} dx e^{ixy} e^{x\alpha} \hat{C}(e^x) \end{aligned} \quad (2.10)$$

We have to require that $e^{x\alpha}\hat{C}(e^x)$ is square integrable, lest we encounter divergent integrals. This is not a very stringent requirement, as we can vary the parameter α to assure convergence. For example, the partition function of the harmonic oscillator

$$Z(\beta) = \frac{1}{2 \sinh \beta/2} \quad (2.11)$$

leads to an L^2 integrable function provided that $\alpha > 1$.

Historically, Eq. 2.10 was first derived for $\alpha = 1$ by Paley and Wiener [21] and then more rigorously by Doetsch [22] for the special case $\alpha = 1/2$. In its form with $\alpha = 1$ it was applied 40 years ago to the analysis of multicomponent exponential decay curves [23]. With the choice $\alpha > 1$ the inversion formula is now amenable to a wider class of functions. Not less important is the fact that a proper choice of this exponent improves the numerical performance of the integrations by an order of magnitude as discussed in Appendix A.

A generalization leading to the multi-dimensional inverse Laplace transform is straightforward, as the main steps in the derivation of formula Eq. (2.10) are based on the Fourier integral. The scalar variables E, β are replaced by N -dimensional vectors $\underline{E}, \underline{\beta}$ to arrive at the N -dimensional inversion formula:

$$\mathcal{C}(\underline{E}) = 2 \frac{e^{\underline{\xi} \cdot (\underline{\alpha} - 1)}}{(2\pi)^N} \operatorname{Re} \lim_{\underline{a} \rightarrow \infty} \int_0^{\underline{a}} d\underline{y} \frac{e^{i\underline{\xi} \cdot \underline{y}}}{\prod_{n=1}^N \Gamma(\alpha_n + iy_n)} \int_{-\infty}^{\infty} d\underline{x} e^{i\underline{x} \cdot \underline{y}} e^{\underline{\alpha} \cdot \underline{x}} \hat{C}(\underline{\beta}), \quad (2.12)$$

where the components of \underline{E} are $(e^{\xi_1}, \dots, e^{\xi_N})$ and $\underline{\beta} = (e^{x_1}, \dots, e^{x_N})$. The components of $\underline{\alpha}$ may be chosen to be different for each degree of freedom.

III. NUMERICAL ANALYSIS

In any numerical application two central questions arise:

- a) How does the accuracy with which $\hat{C}(\beta)$ is known, or which is reduced due to noise, affect the accuracy of the inversion technique?
- b) What is the range of β for which it is necessary to know the Laplace transformed function $\hat{C}(\beta)$ in order to obtain a 'good' representation of the function $\mathcal{C}(E)$?

To answer the first question we will consider in some detail the properties of the inversion formula for a single exponential $\hat{C}(\beta) = e^{-E_0\beta}$. The original signal then is $\mathcal{C}(E) = \delta(E - E_0)$, where $\delta(x)$ is the Dirac ' δ '-function. The function $g(y)$, cf. Eq. 2.7, can be obtained analytically:

$$g(y) = E_0^{-\alpha-iy}\Gamma(\alpha + iy). \quad (3.1)$$

This is a rapidly decaying function in the variable y , since the asymptotic behavior of the Gamma-function for fixed α and large $|y|$ is:

$$|\Gamma(\alpha + iy)| \rightarrow \sqrt{2\pi}|y|^{\alpha-1/2}e^{-\pi|y|/2}. \quad (3.2)$$

The asymptotic behavior of $g(y)$ remains the same, even if the signal is a sum of many exponential terms.

As seen from the exact integration Eq. (3.1), the Gamma-function in the denominator of the inversion formula Eq. (2.10) is cancelled and the y -dependence is simply an oscillating function with constant amplitude. This means that the numerically integrated function $g(y)$ has to be exponentially small in y in order to compensate for the exponentially increasing factor coming from the denominator. The integrand of $g(y)$ as shown in Fig. 1, has an envelope of order unity and due to the term e^{ixy} , it oscillates with increasing frequency as y increases. In the numerical integration, it is necessary to add up many Simpson boxes of height of the order of unity which leads to an exponentially small number $e^{-\pi y/2}$. The boxes have different signs, so for large y this leads to the severe problem of adding many numbers with alternating signs, which differ only by a small amount. At this step we encounter the fact that the inverse Laplace transform is an ill-posed problem: a small error in the signal

$$\hat{C}(\beta) = \langle \hat{C}(\beta) \rangle + \delta\hat{C}(\beta) \quad (3.3)$$

leads to a large error in the integration

$$\langle g(y) \rangle + \delta g(y) = \int K(x, y)(\langle \hat{C}(\beta) \rangle + \delta\hat{C}(\beta)). \quad (3.4)$$

Let m denote the number of decimal digits of the signal and assume that the numerical integrations are all carried out with this same accuracy. Then $g(y)$ can be obtained only up to a certain maximum value

$$y_{\max} \approx \frac{2}{\pi} m \ln 10 \quad (3.5)$$

beyond which any result is meaningless. This implies that the y -integration has to be truncated at y_{\max} . For the single exponent, this leads to the result:

$$\mathcal{C}(E) = \frac{1}{\pi} E^{\alpha-1} E_0^{-\alpha} \frac{\sin(y_{\max} \ln(E/E_0))}{\ln(E/E_0)}, \quad (3.6)$$

which is a function peaked at $E = E_0$ with many side oscillations. An increase of the precision m allows to extend y_{\max} resulting in a narrower peak. In the limit $y_{\max} \rightarrow \infty$ the exact delta function is recovered.

To appreciate this result it is instructive to compare it with an analogous analysis of the Fourier transform of a δ -function. In this case, truncation of the inverse Fourier transform leads to the approximation:

$$\mathcal{C}(E) = \frac{1}{\pi} \frac{\sin(t_{\max}(E - E_0))}{E - E_0} \quad (3.7)$$

If the widths ΔE of these truncated δ -functions are defined as the distance between the first two zeros on each side of the maximum we have for the inverse Laplace transform

$$\Delta_L E = 2E_0 \sinh \frac{\pi}{y_{\max}} \sim E_0 \frac{2\pi}{y_{\max}} \sim E_0 \frac{\pi^2}{m \ln 10}, \quad (3.8)$$

and for the inverse Fourier transform

$$\Delta_F E = \frac{2\pi}{t_{\max}}. \quad (3.9)$$

Whereas for the Fourier integral the width is independent of the position of the approximate delta, this is not true for the inverse Laplace transform. The resolution is automatically higher for lower energy. This means that for a given accuracy m the resolution will increase the lower the energy is.

Now, we come to the second task, the required range of β .

The integrand of $g(y)$ is localized in x : for large negative x , the exponential factor $e^{\alpha x}$ causes the integrand to decay, while for positive x , the exponentially decaying signal itself will also cause the integrand to decay rapidly. The decay for positive x is dependent on the magnitude of the lowest exponent E_0 . If all calculations are performed with a precision of m digits, the value of the function is meaningful only up to the value β_{\max} defined as:

$$e^{-E_0\beta_{\max}} = 10^{-m} \quad \rightsquigarrow \quad \beta_{\max} = \frac{m}{E_0} \ln 10 \quad (3.10)$$

Since the function $g(y)$ is strongly decaying, the sampling theorem [26] assures that the integrand needs to be sampled only at relatively few points. Therefore, the numerical integration involved in obtaining the function $g(y)$ is straightforward. For example, for $\hat{C}(\beta) = e^{-\beta}$, $\alpha = 1/2$, the integrand is larger than 10^{-15} in a range of $\Delta x = 75.0$. Using a Simpson integration rule with step size $h = 0.1$ leads to an integration error of $\sim 10^{-16}$ for $y \in [0, 20]$. That is, we have taken only 750 sampling points for this highly accurate integration, although the integrand varies quite rapidly for $y = 20.0$ with a period of $\Delta_p x = 0.3141$.

In summary, the range of β values needed as well as the resolution with which the inverse transform is performed is determined by the accuracy with which the Laplace transformed function $\hat{C}(\beta)$ can be obtained. The lower the energy of the features, the larger the β range needed but also the higher the resolution. This property will be taken advantage of in the next section to significantly improve the algorithm.

IV. SHIFTING THE LAPLACE TRANSFORM.

Consider the case where the function $\mathcal{C}(E)$ is a sum of δ functions:

$$\mathcal{C}(E) = \sum_{j=0}^{\infty} a_j \delta(E - E_j) \quad (4.1)$$

where the E_j 's are arranged according to ascending order. The Laplace transformed function is

$$\hat{C}(\beta) = \sum_{j=0}^{\infty} a_j e^{-\beta E_j}. \quad (4.2)$$

Define the shifted Laplace transformed function as:

$$\hat{C}(\beta, E_s) \equiv e^{\beta E_s} \hat{C}(\beta). \quad (4.3)$$

The inverse Laplace transform will lead to the function,

$$\mathcal{C}(E, E_s) = \sum_{j=0}^{\infty} a_j \delta[E - (E_j - E_s)], \quad (4.4)$$

where all the eigenenergies have been moved closer to the origin by the amount E_s . As shown in the previous section, such a shift will lead to enhanced resolution in the inverted function.

For illustration, let us consider four exponentials with decay rates 1,2,3,4. In Fig. 2 we plot the inverse transform with a cutoff at $y_{\max} = 5.0$, which means that the accuracy of the signal is only 3 decimal digits. Even the lowest decay rate can hardly be estimated accurately as may be inferred more clearly from a blow-up of the dashed line shown in Fig. 3. The width of the lowest δ -function is of the same order as the spacing and so it is hardly discernible. Shifting the function by $E_s = 0.9$ gives a dramatic increase in resolution. A blow-up of this first peak is provided in Fig. 4. From this figure we can find that the maximum lies at $E = 0.0995$. The price to be paid for the increased resolution is that β_{\max} (cf. Eq. 3.10) must be increased, since it is inversely proportional to the magnitude of the lowest eigenvalue which has now been reduced from E_0 to $E_0 - E_s$. One may now repeat the computation, shifting the data by 0.999 instead of 0.9 and the peak will be resolved with even higher accuracy. In this way, the eigenvalue can be obtained with arbitrary accuracy.

V. NUMERICAL APPLICATIONS

A. Partition function of the harmonic oscillator

The exact inversion of the partition function Eq. (2.11) leads to a train of delta functions at the positions of the eigenvalues of the harmonic oscillator. This function was chosen

because its numerical Laplace inversion belongs to the most difficult class of problems. A non-linear least-squares method (without any knowledge in advance) could fit at most five exponentials. On the other hand, expansions in different basis sets converge too slowly [2]. The inverse Laplace transform of the partition function was computed with different degrees of decimal digits precision. Fig. 5 compares calculations with double precision, i.e. 15 decimal digits, and a little higher accuracy, 26 decimal digits. Whereas for double precision only the two lowest eigenvalues can be identified, at the higher accuracy the four lowest eigenvalues are resolved.

The results of pushing the accuracy to 60 and 105 decimal digits precision are shown in Fig. 6. At 105 decimal digit precision it is possible to identify the eigenvalues up to the 10th level. The range of β values used in all these computations is as in Eq. (3.10), $\beta_{\max} \approx 4.5m$. Of course, these calculations cannot be applied to data obtained from a Monte Carlo computation. However, as also discussed in the next section, they may be used to invert basis sets which can then be fitted to Monte Carlo data. These results also serve to demonstrate the relative simplicity and accuracy of the method and the fact that in principle it will work for any number of peaks.

To test the noise-sensitivity of the inverse Laplace transform, we added to the signal a Gaussian distributed noise with zero mean and different levels of RMS deviation σ . The signal is assumed to be given up to $x = 5.52$, i.e. $\beta_{\max} = 250$. Fig. 7 shows that beyond the cut-off value y_{\max} there is an accumulation of numerical errors and the signal deviates from a cosine-like wave. This Figure also confirms that the cut-off value depends rather linearly on the logarithm of the RMS deviation of the noise σ . In Fig. 8, the signal is shifted to the left by $E_s = 0.4$, so that the smallest decay rate is around $E \approx 0.1$. The cut-off values change only slightly under the shift operation, but the integrand contains more oscillations before the cut-off, leading to an enhanced resolution in the peaks.

B. Reflection probabilities

The Laplace transform of the reflection probability for the Eckart potential [28],

$$R(E) = \frac{1 + \cosh(\sqrt{4\alpha^2 - \pi^2})}{\cosh(2\alpha\sqrt{E/V^\dagger}) + \cosh(\sqrt{4\alpha^2 - \pi^2})}, \quad (5.1)$$

see Fig. 9, is computed by numerical integration. Then the real inversion formula Eq. (2.10) is used to regain the reflection probability. The difference between the exact function and the inverted one for the parameter choice $\alpha = 4.0, V^\dagger = 5.0$ is too small to be seen by the naked eye. A blow-up of the error is shown in Fig. 10. Even for the rather low accuracy of only 3 decimal digits the relative error is about 10^{-2} , and as seen from the Figure, it decreases with increasing precision of the data. For the parameter $\alpha = 12.0, V^\dagger = 5.0$ the results are a bit worse, as shown in Fig. 11, due to the ‘Gibb’s phenomenon’ [29]. Near the step, $E \approx 5.0$ the error increases significantly.

In all the computations the cut-off y_{\max} was chosen to minimize the error: decreasing the value of y_{\max} reduces the resolution but increasing it leads to numerically wrong values due to the uncertainty of the signal. In Fig. 12 we show a typical integrand $\text{Re}\{g(y)/\Gamma(1/2 + iy)\}$: if the inverse Laplace transform is not known, it is easy to judge which value for y_{\max} has to be chosen, as the integrand decays smoothly and then produces artificial oscillations and blows up. (For an exact step transmission probability $\hat{f}(\beta) = \frac{1}{\beta}e^{-V^\dagger\beta}$, the integrand goes asymptotically to 0 as $1/(\alpha - 1 + iy)$.)

C. Below-barrier resonance

A small resonance in the form of a Lorentzian is added to the transmission probability

$$T(E) = \frac{\varepsilon^2}{(E - E_0)^2 + \varepsilon^2} + \frac{\cosh E/V_0 - 1}{\cosh E/V_0 + a}, \quad (5.2)$$

with parameters given in Fig. 13. The accuracy of the data is 10^{-6} and the features are reproduced quite well. The oscillations at very low energy are side oscillations of the resonance and it is possible to smooth them away. As outlined above, the resolution depends

on the energy of the feature. In order to reproduce a Lorentzian of width ε , it is necessary to have at least a comparable resolution. To check whether the Lorentzian coming out of the inversion is broadened because of lack of resolution, the signal can be shifted towards lower energy.

In this example we took the Laplace transform of the reflection probability with $\beta_{\max} = 10^6$. One may also use the transmission probability, however it diverges at $\beta = 0$ and so this requires some care.

VI. DISCUSSION

In this paper we have resurrected and generalized a formula of Doetsch which enables a direct Laplace inversion of a large class of functions. By suitable scaling, these can include functions that are not L^2 integrable. Therefore the algorithm is directly applicable to partition functions, for example. The method is relatively simple, all that is needed are two fast Fourier transforms. It is not necessary to pre-smooth the data. The method is controllable, the more accurate the Laplace inverted data, and the larger the range, the more accurate are the inversion results. The parameters of the inversion are controlled by the accuracy of the data only. As a result, the method is stable with respect to small perturbations.

We have shown that in practice, an extremely high quality inversion can be obtained provided that the signal is also of very high accuracy. This is not merely an academic exercise. For example, the Laguerre basis set may be taken, systematically inverted, and the resulting numerical functions may be stored. Then the Laplace transformed function may be expanded in terms of Laguerre polynomials. The inverted function is then obtained merely by reading off the inverted Laguerre functions. The utility of such a procedure depends on the quality of the fit of the polynomials to the numerical Laplace transformed data. It may be, that more sophisticated techniques should be used which include local smoothing of the data, such as the DAFS methodology [33]. In any case, once the Laplace transformed data is projected onto standard basis sets, the high accuracy inversion may be

used to obtain the inverted function.

An important property of the inversion technique is the fact that the resolution of the resulting signal depends on the location of the signal. The closer it is to the origin, the higher is the resolution. This allows for a shifting of the signal to obtain an increased resolution. The price to be paid is that each shift demands knowledge of the function for larger values of β . For analytic functions, such as the Laguerre polynomials, this does not present any severe difficulty, as present day computers enable computations with very high accuracy, which is also demonstrated for the harmonic oscillator partition function.

The Laplace inversion method presented in this paper is ideally suited for data obtained from matrix multiplication schemes [31,32]. These methods produce the data at points $\beta_j = \Delta\beta 2^j$ [30], while the inversion requires $\beta_j = e^{j\Delta x}$.

In this paper we have not considered correlation functions. Elsewhere [34] we will present the application of the present method to spectra and correlation functions. In principle there is no special complication except for the fact that in some cases a two dimensional inverse Laplace transform has to be computed.

We have also not considered directly the numerical analytic continuation of functions. As already mentioned in the Introduction, once the inverted function is obtained, it may be Fourier transformed to obtain the analytically continued function. In this sense, the inversion technique presented in this paper may be thought of as a representation of the complex valued Dirac δ function. The real question is one of practical usage, that is the level of accuracy needed to obtain the real time function from the imaginary time function as well as the range of β values needed for a given time length. Other applications are the computation of moments of a probability distribution from its transform [35]. These questions will be considered in future studies [34].

Acknowledgements

B. H. gratefully thanks the MINERVA foundation, Munich, for a grant and the Weizmann Institute of Science for its hospitality. This work has been supported by grants from the

US-Israel Binational Science Foundation and the Israel Science Foundation.

APPENDIX A: OPTIMIZING THE CHOICE OF α

We will outline how the parameter α can help reduce the numerical effort drastically, especially in high precision calculations.

The main numerical advantage of introducing α is a shortening of the integration interval in x needed for obtaining $g(y)$, cf. Eq. (2.7). The range of integration $[x_{min}, x_{max}]$ is determined by the required accuracy $\varepsilon = 10^{-m}$. The negative limit is mainly fixed by the exponential $e^{\alpha x}$,

$$x_{min} = \frac{1}{\alpha} \ln \frac{\varepsilon}{\hat{C}(0)}, \quad (6.1)$$

and the positive limit is due to the very rapid decay of $\hat{C}(e^x)$ which is almost independent of α and is determined by the smallest decay rate. The larger α , the smaller the integration interval, but if α becomes too large the integrand increases exponentially, magnifying uncertainties in the signal.

The maximum value of the integrand, if one exponential decay $\hat{C}(\beta) = a_0 e^{-E_0 \beta}$ is considered, is at $x_m = \ln \alpha / E_0$ and the integrand $I(x)$ takes the value

$$I(x_m) = a_0 e^{\alpha(\ln \alpha / E_0 - 1)} \approx a_0 e^{\alpha \ln \alpha}, \quad (6.2)$$

which goes essentially as $\alpha!$. The larger α , the more digits are required in the computation. On the other hand, the outcome of the integration must cancel the denominator $\Gamma(\alpha + iy)$ whose large y -asymptotics is given by Eq. (3.2). For a given y_{max} the order of magnitude of $\Gamma(\alpha + iy)$ divided by the integrand at $y = 0$, $\Gamma(\alpha) \approx \alpha^\alpha \approx e^{\alpha \ln \alpha}$ has to be comparable to the given accuracy $\varepsilon = 10^{-m}$:

$$\frac{y_{max}^{\alpha-1/2} e^{-\pi y_{max}/2}}{(\alpha-1)!} = \frac{\varepsilon}{a_0} \quad (6.3)$$

In summary, for large cut-off values y_{max} the stepsize in the x integration remains approximately the same. A change of α reduces the interval of the first integration, but to

keep the same resolution (i.e. keep y_{max} fixed) it is necessary to increase the precision m . We found that for $m \approx 100$, $\alpha \approx 10$ is a reasonable choice.

REFERENCES

- [1] D. K. Cope, *SIAM J. Num. Anal.* **27**, 1345-1354 (1990)
- [2] B. Davies and B. Martin, *J. Comput. Phys.* **33**, 1-32 (1979)
- [3] M. Jarrell and J. E. Gubernatis, *Phys. Rep.* **269**, 133 (1996)
- [4] H. Dubner and J. Abate, *J. Assoc. Comput. Mach.* **15**, 92 (1968); J. Abate and H. Dubner, *SIAM J. Numer. Anal.* **5**, 102 - 112 (1968); H. Dubner, *Math. of Comput.* **58**, 729-736 (1992)
- [5] G. Doetsch, *Laplace Transformation*, Dover (1943)
- [6] R. Piessens, *J. Inst. Math. Appl.* **10**, 185-192 (1972)
- [7] A. Papoulis, *Quart. Appl. Math.* **14**, 405-414 (1956)
- [8] S. W. Provencher, *J. Chem. Phys.* **64**, 2772 - 2777 (1975)
- [9] L. Schlessinger, *Phys. Rev.* **167**, 1411-1423 (1967)
- [10] H.-B. Schüttler and D. J. Scalapino, *Phys. Rev. B* **34**, 4744 - 4756 (1986)
- [11] J. R. Rice, *The approximation of functions*, Addison Wesley (1969)
- [12] D. Braess, *Computing* **2**, 309-321 (1967)
- [13] M. Bertero, P. Brianzi, E. R. Pike, and L. Rebolia, *Proc. R. Soc. Lond. A* **415**, 257 (1988)
- [14] P. Linz, *Inverse Probl.* **10**, L1 (1994)
- [15] A. N. Tikhonov and V. Y. Arsenin, *Solutions of ill-posed problems*, Halsted Press, Wiley (1977)
- [16] J. E. Gubernatis, M. Jarrell, R. N. Silver, and D. S. Sivia, *Phys. Rev. B* **44**, 6011 (1991)
- [17] E. Gallicchio and B. Berne, *J. Chem. Phys.* **101**, 9909 (1994)
- [18] E. Gallicchio and B. Berne, *J. Chem. Phys.* **104**, 7064 (1996)
- [19] Dongsup Kim, J. D. Doll, and J. E. Gubernatis, *J. Chem. Phys.* **106**, 1641 (1997)
- [20] S. A. Egorov, E. Gallicchio, and B. J. Berne, *J. Chem. Phys.* **107**, 9312 (1997)
- [21] R. Paley and N. Wiener, *Amer. Math. Soc. Colloquium Publ.* **19** (1934)
- [22] G. Doetsch, *Math. Zeitschr.* **42**, 263-286 (1937)

- [23] D. G. Gardner, J. C. Gardner, and W. W. Meinke, *J. Chem. Phys.* **31**, 978 - 986 (1959)
- [24] G. Doetsch, *Math. Zeitschr.* **41**, 283-318 (1936)
- [25] M. Abramowitz and I. A. Stegun, *Pocketbook of Mathematical Functions*, Harri Deutsch, (1984)
- [26] C. E. Shannon, *Communication in the Presence of Noise*, *Proc. IRE*, January (1949)
- [27] W. H. Press, S. A. Teukolsky, W. T. Vetterling, and B. P. Flannery, *Numerical Recipes: The Art of Scientific Computing*, 2nd ed., Cambridge (1992)
- [28] H. S. Johnston and D. Rapp, *J. Am. Chem. Soc.*, **83**, 1 (1961)
- [29] A. Papoulis, *The Fourier integral and its applications*, McGraw-Hill, New York (1962)
- [30] R. P. Feynman and A. R. Hibbs, *Quantum Mechanics and Path Integrals*, McGraw-Hill, New York (1965)
- [31] R. G. Storer, *J. Math. Phys.* **9**, 964 (1968)
- [32] D. Thirumalai, E. J. Bruskin, and B. Berne, *J. Chem. Phys.* **79**, 5063 (1983)
- [33] D. K. Hoffman, G. W. Wei, D. S. Zhang, and D. J. Kouri, *Chem. Phys. Lett.* **287**, 119-124 (1998)
- [34] B. Hüpper and E. Pollak, work in progress.
- [35] G. L. Choudhury and D. M. Lucantoni, *Operations Research* **44**, 368 - 381 (1996)

FIGURES

FIG. 1. Integrand of the inverse Laplace inversion formula for a signal of one exponential decay. The envelope is decaying exponentially for $x \rightarrow -\infty$ and even more rapidly for $x \rightarrow +\infty$. The rapid oscillations result in an exponentially small value $g(20) \approx 5 \cdot 10^{-14}$ of the integral although the integrand is of the order of unity.

FIG. 2. Inverse Laplace transform of a sum of four exponential decays with decay rates $E_n = 1, 2, 3, 4$. The accuracy of the signal is taken as 3 decimal digits. The inversion of the original data allows at most the estimation of the first delta function (dashed line) at $E = 1$. The solid line shows the inversion of the data shifted by $\delta E = 0.9$ to the left. The first maximum can now be estimated much more accurately.

FIG. 3. Magnification of the unshifted inversion of Fig. 2. The exact curve should yield a delta function at $E = 1.0$. Due to the insufficient accuracy of the data, the four components overlap and distort the maximum to $E \approx 1.05$.

FIG. 4. Magnification of the shifted inversion Fig. 2. The exact curve should yield a delta function at $E = 0.1$. This value may now be estimated very accurately from the shifted data, even though the accuracy ($m = 3$) is low.

FIG. 5. Numerical inverse Laplace transform for the partition function of the harmonic oscillator. The exact inverse should yield $\sum_n \delta(E - (n + 1/2))$. The two lines correspond to different input signals whose accuracy (significant decimal digits) is indicated in the insert. The value of $\alpha = 4$ was used for all computations with the harmonic oscillator partition function.

FIG. 6. High precision numerical inverse Laplace transform for the partition function of the harmonic oscillator. Other notation is as in Fig. 5.

FIG. 7. Noisy data. The integrand of the real inversion formula for the partition function of the harmonic oscillator is plotted vs. y . Gaussian noise with RMS deviation σ as indicated is added to the signal and this leads to a reduction of the cut-off value for the y -integration.

FIG. 8. Noisy shifted data. The data used for Fig. 7 are shifted by $E_s = 0.4$ to the left. The cut-off values in y remain the same, but because of the faster oscillation of the integrand, the resolution of the final inversion peaks will be increased.

FIG. 9. Reflection probabilities for the Eckart barrier with two different choices of the parameters. For all reflection probabilities we used $\alpha = 0.5$.

FIG. 10. Logarithm of the error of the inverted reflection probability of the Eckart potential with $\alpha = 4.0, V^\ddagger = 5.0$. The signal for the inversion is obtained by numerical Laplace transform of the exact reflection probability and the accuracy in decimal digits of the numerical Laplace integral is indicated. The values for y_{\max} are 5.5 and 12.0 for 3 and 8 digits accuracy respectively.

FIG. 11. Logarithm of the error of the inverted reflection probability of the Eckart potential with $\alpha = 12.0, V^\ddagger = 5.0$. Other notation is as in Fig. 10. The error increases near the step at $E = 5.0$ due to Gibb's phenomenon.

FIG. 12. Integrand of the real inversion formula for the Eckart barrier reflection probability at $\alpha = 4.0, V^\ddagger = 5.0$. The integrand is expected to decrease like $1/(c + iy)$, but beyond the cut-off $y_{\max} \approx 12.5$ artificial oscillations arise and the integrand blows up.

FIG. 13. Numerical inverse Laplace transform for a below barrier resonance added to the reflection probability of the Eckart barrier $T_{res}(E) = \varepsilon^2/((E - E_0)^2 + \varepsilon^2)$, with $\varepsilon = 0.013, E_0 = 0.05$, added to the transmission probability $T(E) = (\cosh 20E - 1)/(100 + \cosh 20E)$. The accuracy of the data is 6 decimal digits.

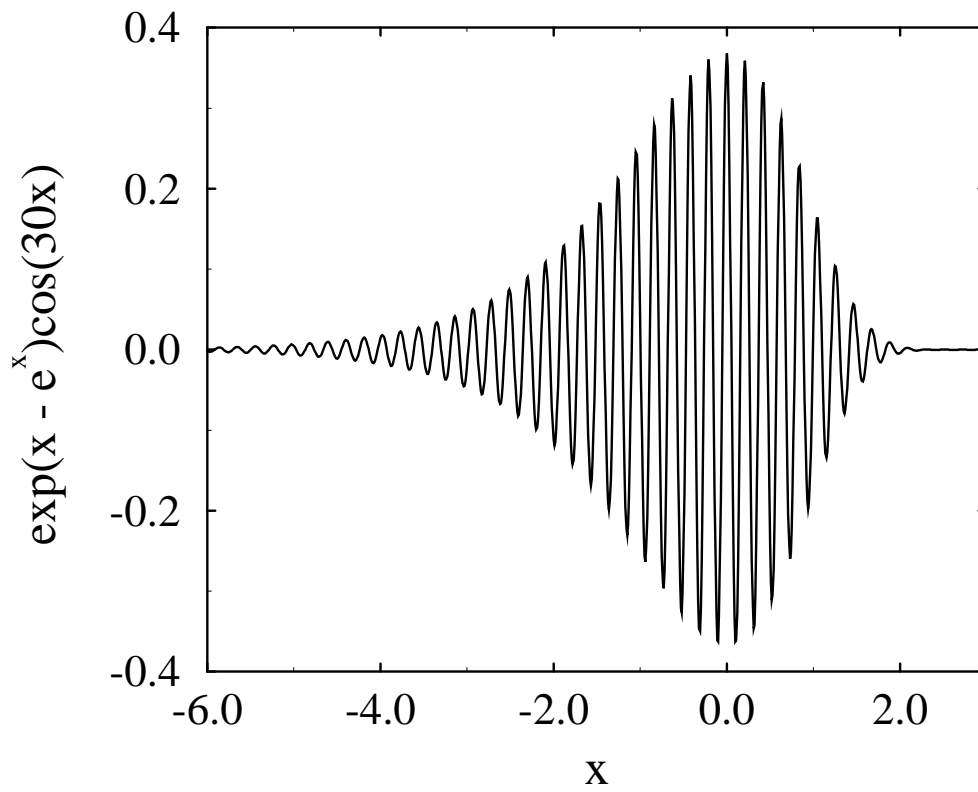


Fig. 1

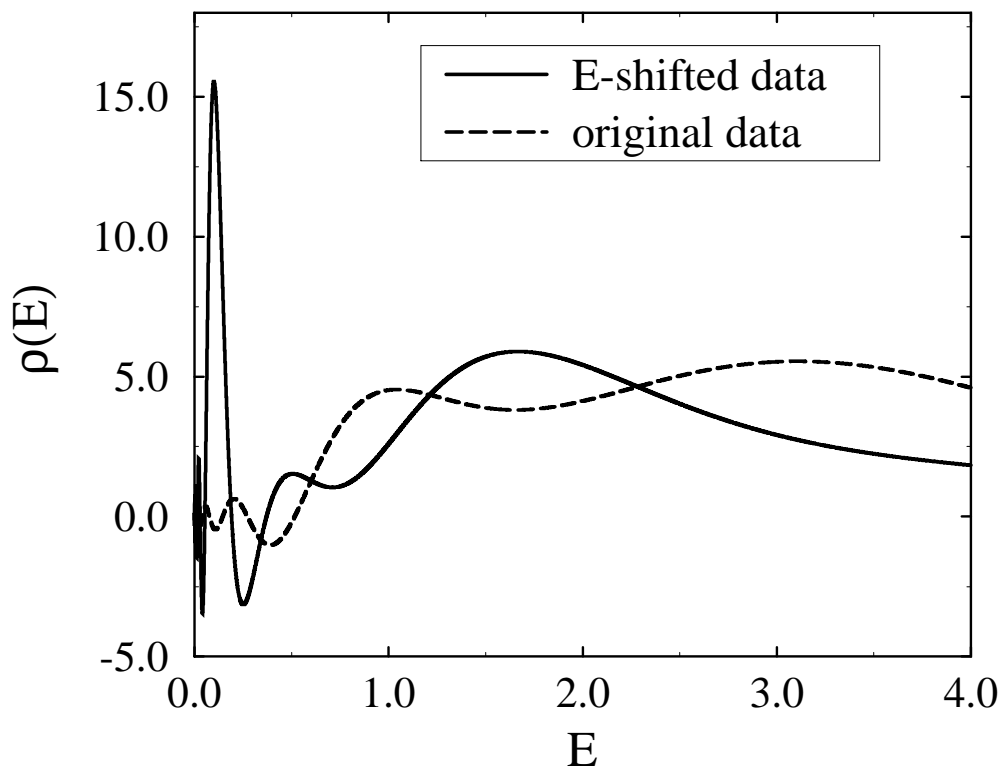


Fig. 2

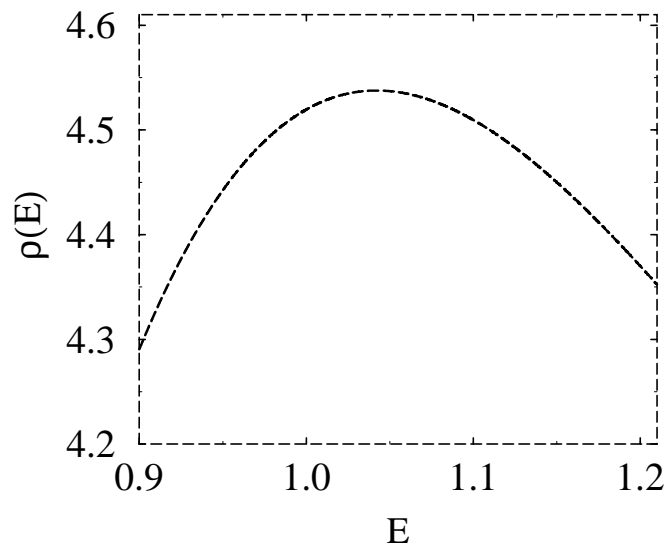


Fig. 3

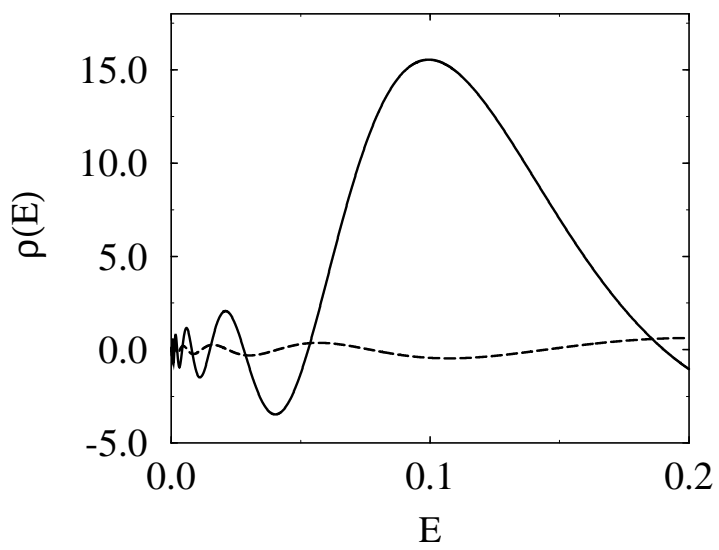


Fig. 4

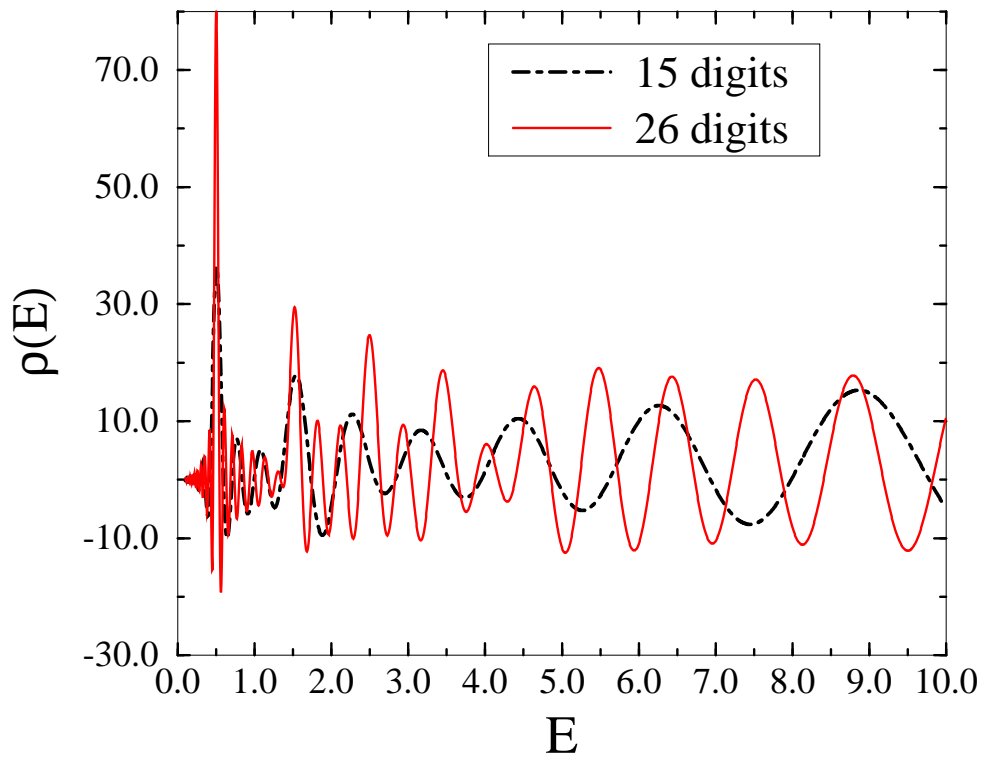


Fig. 5

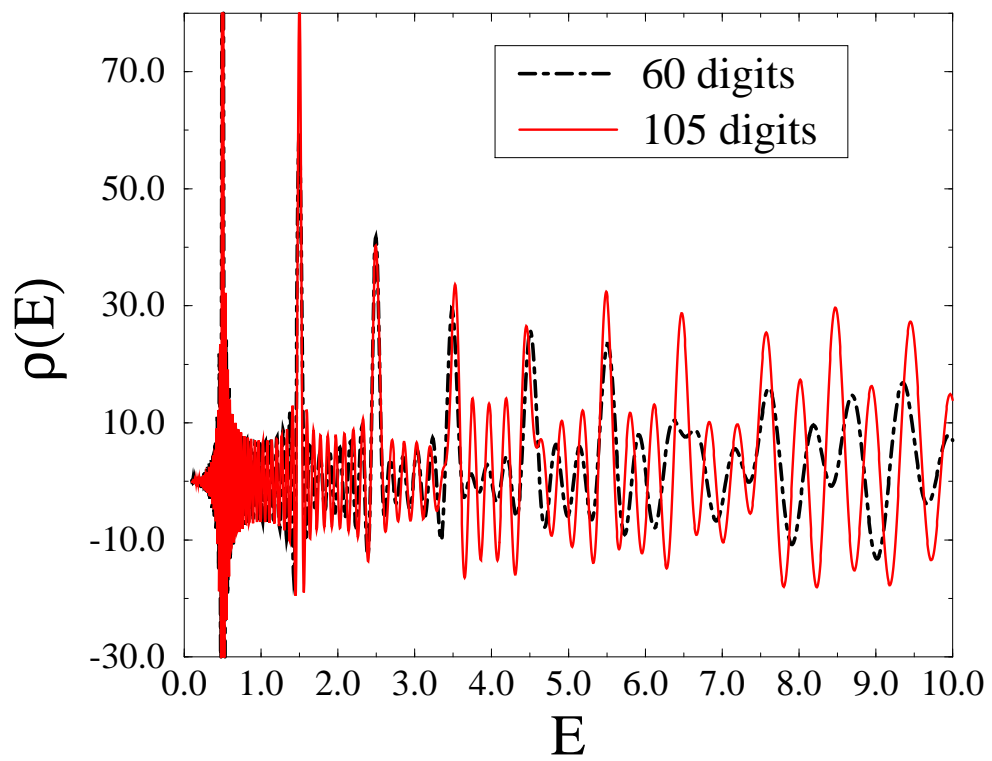


Fig. 6

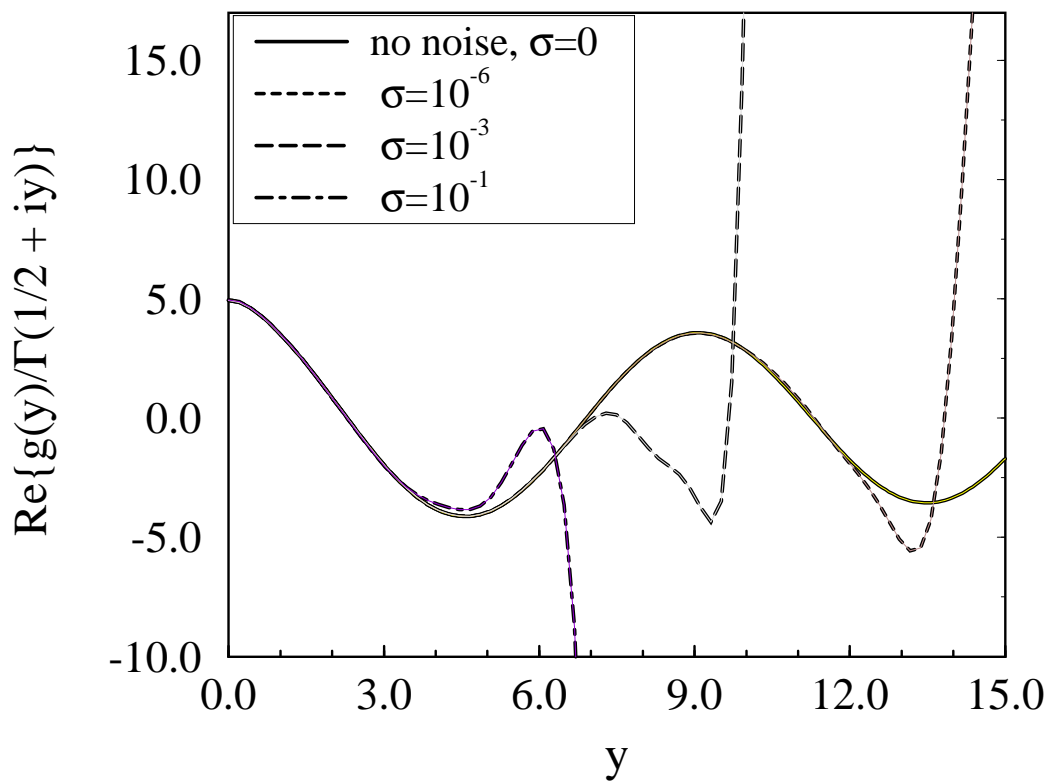


Fig. 7

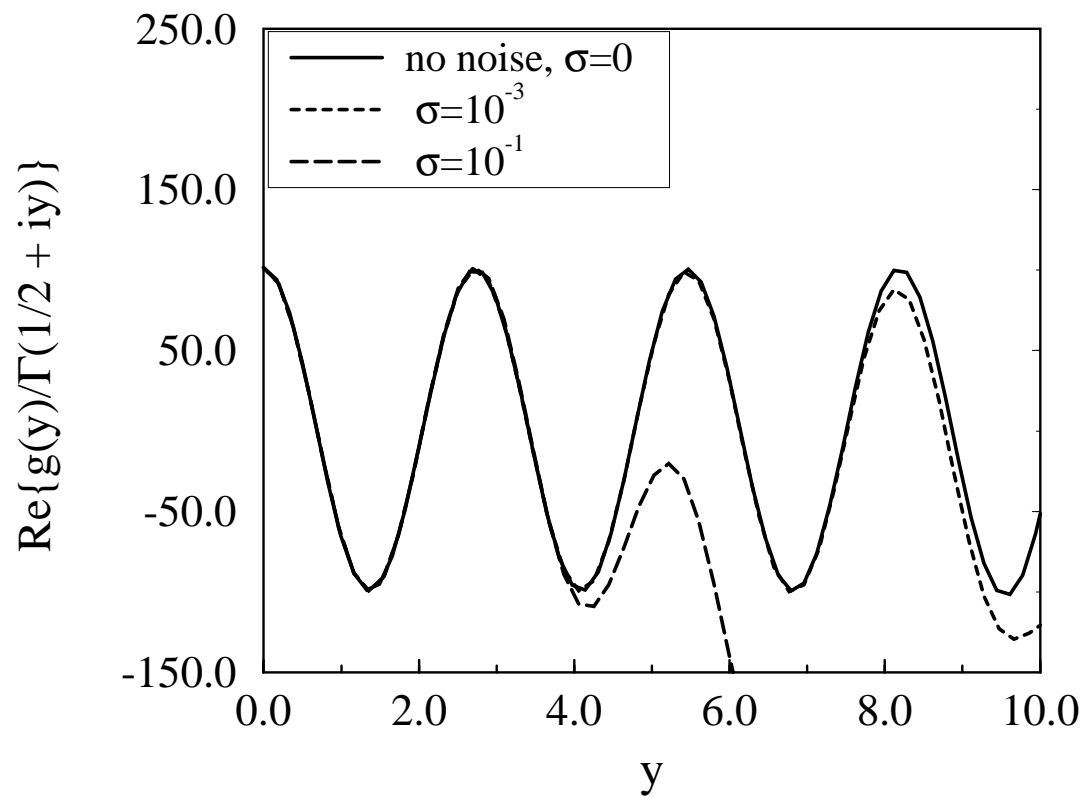


Fig. 8

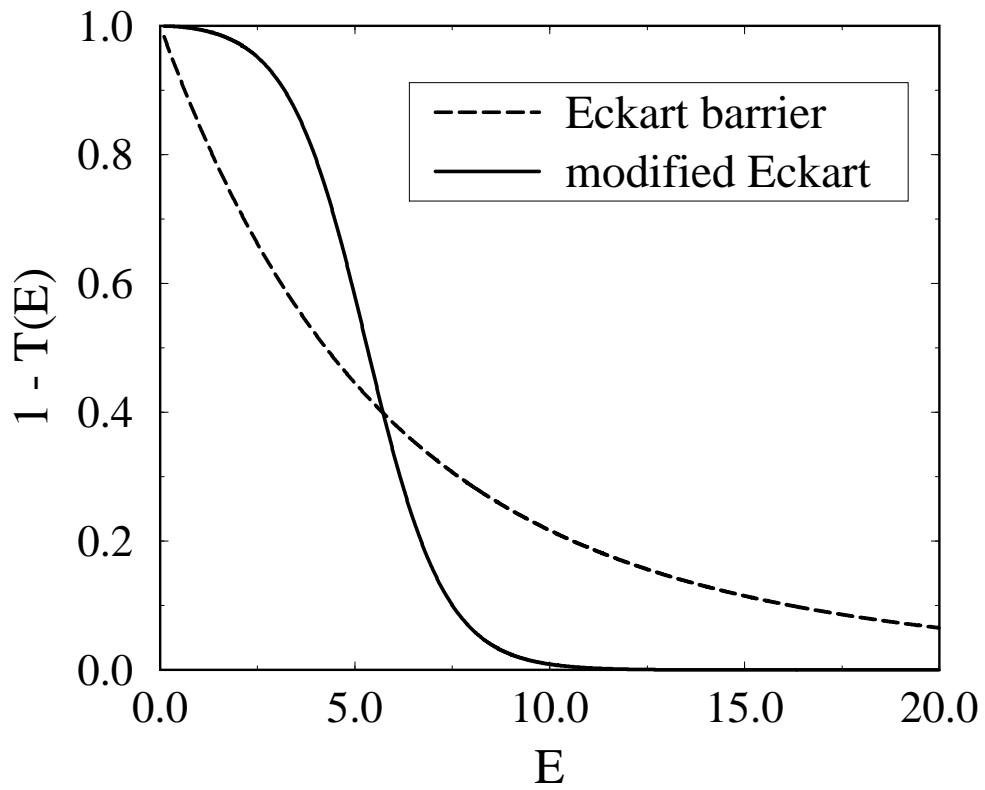


Fig. 9

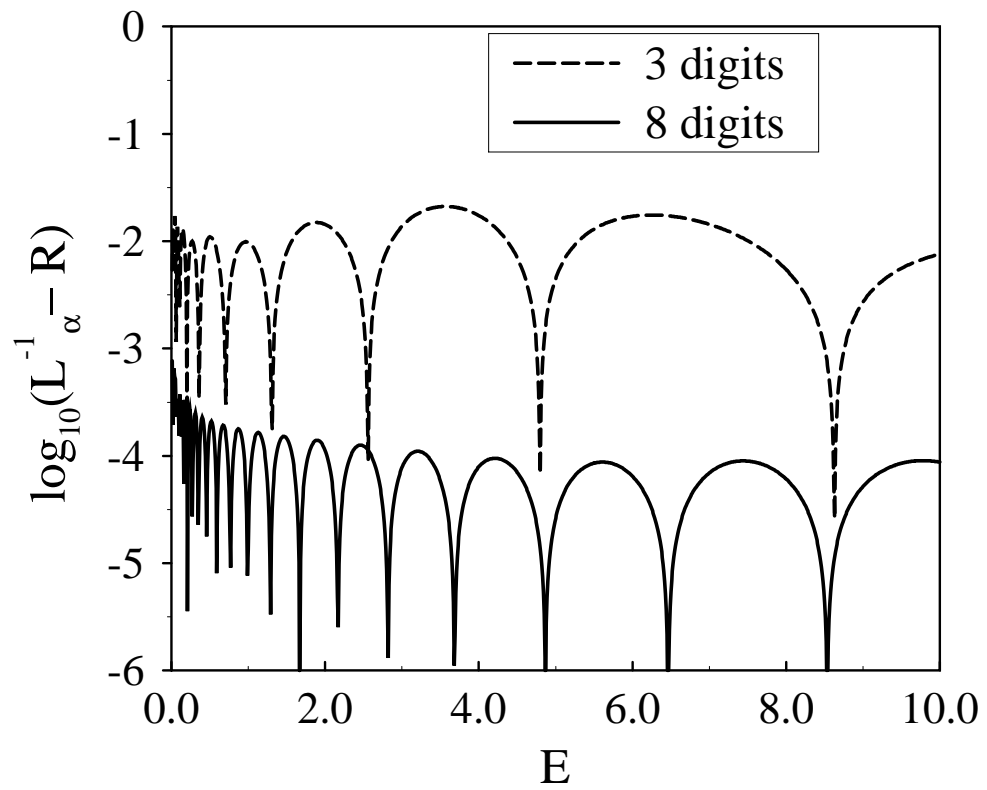


Fig. 10

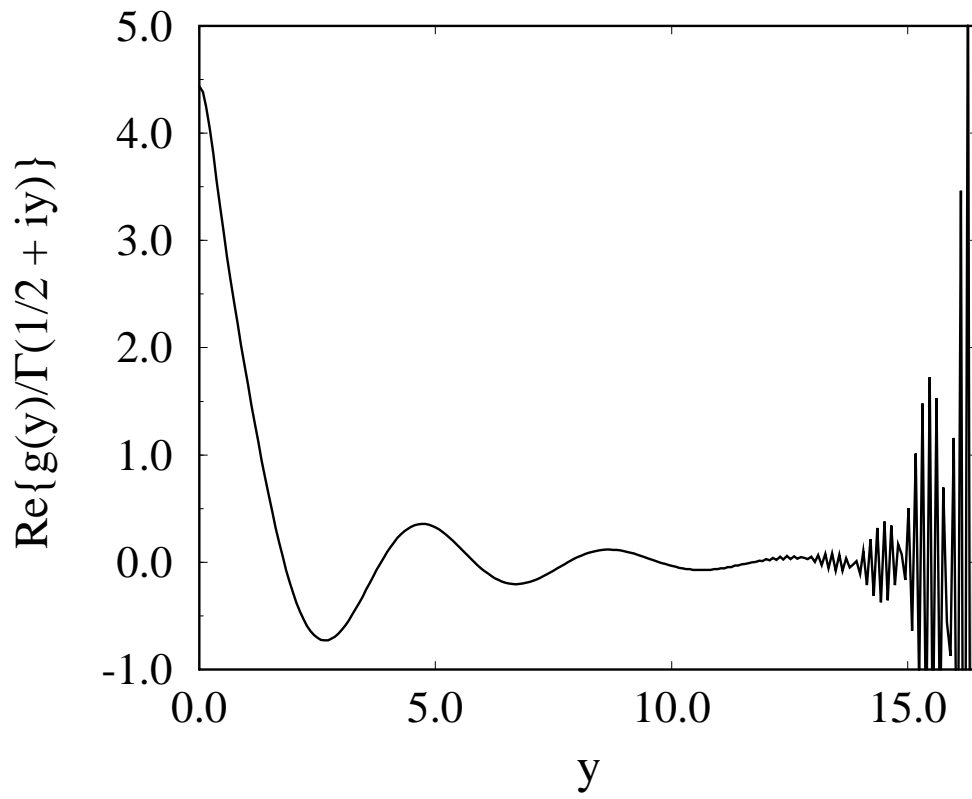


Fig. 12

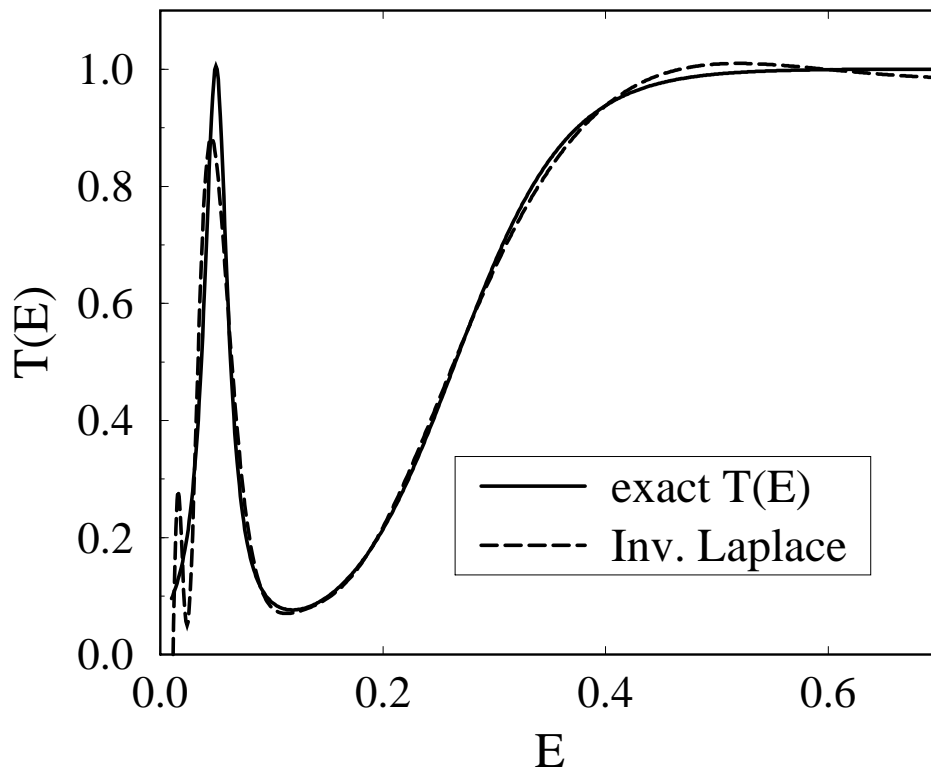


Fig. 13